DOI: 10.61782/fa.2025.0760

FORUM ACUSTICUM EURONOISE 2025

ROTATABLE PHONONIC CRYSTAL WITH MULTIRESONANT SCATTERERS FOR ACOUSTIC SWITCHING APPLICATIONS

David Ramírez-Solana[1,2,3,4*] **Valentino Sangiorgio**[2,3] **Rubén Picó**[2]
Javier Redondo[2] **Muhammad Gulzari**[1] **Maria Pia Fanti**[4]
[1] Structured Materials and Dynamics Lab, School of Civil Engineering, University College Dublin, Ireland
[2] Instituto de Investigación para la Gestión Integrada de Zonas Costeras, Universitat Politècnica de València, Gandía, Spain
[3] Department of Engineering and Geology (INGEO), D'Annunzio University of Chieti-Pescara, Pescara, Italy
[4] Department of Electrical and Information Engineering, Politecnico di Bari, Bari, Italy

ABSTRACT

This study presents an acoustic switch based on a sonic crystal (SC) with multiresonant scatterers arranged in a square 2D lattice. The scatterers feature Helmholtz resonators (HRs) tuned to different frequencies. A 90° rotation of all scatterers enables switching the interaction between Bragg bandgaps (Bragg- BGs) and Helmholtz resonator (HR) bandgaps, creating selective frequency filtering and wave propagation control. The research targets low to mid frequencies (500-2500 Hz), an underexplored range in current studies. The structure, made via cost-effective 3D printing without infill to reduce absorption, is both simple and practical. Tests in an anechoic chamber reveal a notable 20 dB contrast in acoustic insulation. This design offers potential applications in noise reduction for urban and industrial settings, adaptive acoustic systems, sensors, and acoustic energy harvesting.

Keywords: *Acoustic Switch, Helmholtz Resonators, Multiresonant Scatterer.*

**Corresponding author*: *david.ramirezsolana@ucd.ie.*

1. INTRODUCTION

Phononic crystals are periodic structures composed of rigid scatterers embedded in a fluid. A particular case of phononic crystals is the so-called Sonic Crystals (SCs), where the fluid is air. They allow fluid and light passage while blocking specific acoustic frequencies due to multiple scattering effects [1]. These frequency gaps, known as Bragg Bandgaps (Bragg-BGs) [2], depend on the lattice periodicity. The first Bragg-BG for a square lattice under normal incidence occurs at $f_{\text{Bragg}} = c/2a$, where c is the sound speed in air and a is the lattice parameter [3].

SCs have been extensively studied since Kock and Harvey's pioneering work [1], enabling applications in waveguides [4], diffusers [5], noise barriers [6, 7], and switches [8]. Beyond Bragg scattering, local resonances, particularly from Helmholtz resonators (HRs) [9], create additional bandgaps (HRs-BGs). Their frequencies depend on the internal cavity and mouth orientation, offering enhanced wave control [10, 11].

Most acoustic metamaterials operate passively within fixed frequency ranges, limiting adaptability [12]. Phononic crystals with asymmetric scatterers have demonstrated switching capabilities in high-frequency regimes (around 300 kHz) by independently varying scatterer angles [13].

This study introduces a multiresonant SC-based acoustic switch. Each scatterer consists of two perpen-

dicular HRs, enabling two distinct configurations: 0° and 90°, relative to the incident wave. These orientations determine selective frequency filtering by tuning Bragg- and HRs-BGs. The switch functionality requires mechanical adjustment of all scatterers.

The paper is structured as follows: Section Fig. 2 details the methodology, covering numerical modeling (II.A), 3D printing (II.B), and experimental validation (II.C). Section Fig. 3 presents numerical and experimental comparisons, assessing the device's performance. Finally, Section Fig. 4 summarizes key findings and practical applications.

2. MATERIALS AND METHODS

We analyze a 2D sonic crystal (SC) composed of scatterers with Helmholtz resonators (HRs) arranged in an infinite periodic square lattice. The unit cell, illustrated in Fig. 1a, consists of a scatterer with an outer radius R and two apertures forming HRs with distinct resonant frequencies. Periodic boundary conditions are applied along the X and Y boundaries to model the infinite SC, characterized by a constant square lattice parameter a and the unit cell of the irreducible Brillouin zone in reciprocal space [14]. The HRs are defined by the neck length L (thickness and difference between outer and inner radii), mouth width w, and inner surface area S. The first resonant frequencies of the HRs oriented at 0° and 90° are given by [15]:

$$f_{HR}^{0°/90°} = \frac{c}{2\pi}\sqrt{\frac{w}{(L+\delta\frac{w}{2})S_{0°/90°}}} \tag{1}$$

where δ is the correction factor for the effective neck length, accounting for the neck-cavity junction effects due to sudden changes in circular cross-sections (typically between 1.6 and 1.8).

The first resonances of the HRs ($f_{\text{HR}}^{0°}$ and $f_{\text{HR}}^{90°}$) relative to the central frequency of the Bragg bandgap (f_{Bragg}) are critical in determining their interaction with the periodic structure. Notably, the inclusion of HRs in an SC does not inherently reduce transmission through the structure [11]. Therefore, careful attention must be given to the alignment of the HR mouths and their fundamental frequencies. Fig. 1a depicts a scatterer with two HRs aligned at 0° and 90°, with coupled surfaces and a 110° angle between the separation walls. The central frequency of the Bragg bandgap is $f_{\text{Bragg}} = 1400$ Hz, with the HRs' fundamental frequencies at the extremes of the first Bragg bandgap. The larger cavity (90°) has $f_{\text{HR}} = 760$ Hz $> f_{\text{Bragg}}$, while the smaller cavity (0°) has $f_{\text{HR}} = 1800$ Hz $< f_{\text{Bragg}}$. Both HRs share identical mouth dimensions ($w = 0.025$ m) and neck length ($L = 0.006$ m).

Thermoviscous losses in the medium are negligible in this study due to the dimensions of the multiresonant scatterers and the low frequency range of interest (see Appendix A in ref [11]). At a measurement temperature of 293 K and the lowest operational frequency of 500 Hz, the viscous and thermal boundary layers in air are calculated to be 116 μm and 97.8 μm, respectively. These values are 1.56% and 1.85% of the neck length $L = 0.006$ m, well below the 5% threshold known to affect acoustic performance in small cavities [16].

The band structure is calculated for different propagation directions (ΓX, XM, MX', $X'\Gamma$), as shown in the inset of Fig. 1a. These directions correspond to the unit cell of the SC and the irreducible Brillouin zone of the square lattice, based on Bloch-Floquet theory [14]. Numerical simulations evaluate transmission in two configurations: ΓX for the 0° orientation and $X'\Gamma$ for the 90° orientation. Periodic boundary conditions (PBC) are applied along the Y-direction to emulate an infinite SC, while the X-direction is limited to three rows of scatterers for practical modeling (see Fig. 1b and Fig. 1c).

Both transmission models use a lattice parameter $a = 0.12$ m. The geometric model of the SC and the unit cell represent the same periodic structure, a 2D square lattice. However, while the unit cell represents an infinite system, the transmission models consist of three-layer systems with infinite lateral extension. A harmonic plane wave with frequency f and acoustic pressure P_i propagates along the X-axis, aligned with the mouth of the higher-frequency HR in Fig. 1b and the lower-frequency HR in Fig. 1c (referred to as 0° and 90° alignments). Perfectly matched layers (PML) are placed at the ends of the X-axis to absorb outgoing waves.

Transmission is determined using pressure fields (P_t) evaluated at specific points (shown in Fig. 1b and Fig. 1c), positioned 1 m from the SC. Fig. 1d shows a numerical model simulating the experimental setup described in Section 2.2. This 2D simulation replicates expected experimental conditions, enabling direct comparison between numerical predictions and experimental results. The evaluation region is defined by a grid with points spaced at intervals of $a/4 = 0.03$ m, allowing accurate analysis of the transmitted pressure field in the frequency range of interest.

In Fig. 1d, the source is represented by a vertical line emitting an acoustic pressure of 1 Pa, located 0.5 m from the nearest scatterers. The evaluation region spans 0.5 m

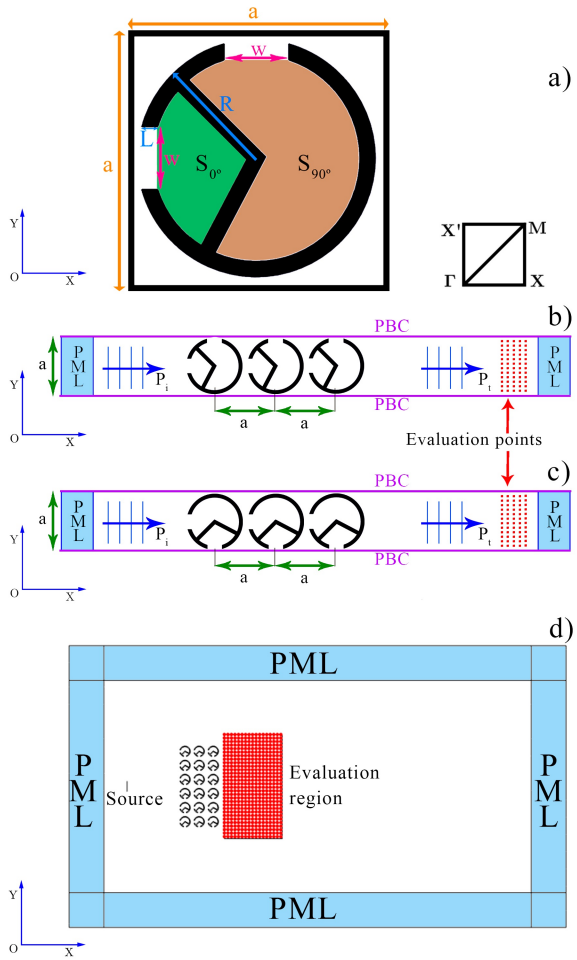

Figure 1. (a) Unit cell with two Helmholtz resonators; inset shows paths in the irreducible Brillouin zone. (b) and (c) Transmission models for 0° and 90° orientations. (d) Full numerical model corresponding to the experimental setup.

along the x-axis and 1.1 m along the y-axis, with the closest measurement points 0.05 m from the last scatterer row and the furthest points 0.55 m away. The y-axis evaluation region is centered relative to the SC array (3 columns by 6 rows), leaving 0.09 m between the evaluation region and the top and bottom edges of the SC structure.

Transmittance ($\mathbb{T}$) is defined as:

$$\mathbb{T} = \frac{\langle P_{t,with}^2 \rangle}{\langle P_{t,without}^2 \rangle} \tag{2}$$

where $\langle\rangle$ denotes the average over all evaluation points, $P_{t,without}$ is the acoustic pressure without the SC, and $P_{t,with}$ is the transmitted acoustic pressure with the SC. Insertion loss (IL) in decibels is derived from Eq. 2:

$$\text{IL} = -10 * \log_{10}(\mathbb{T}), \text{ [dB]} \tag{3}$$

This equation quantifies the change in sound pressure level (SPL) at the evaluation points when the SC is placed in the path of the incident acoustic wave.

The transmission coefficient $\mathbb{T}$ is used to compare the performance of the SC configurations across different frequency ranges. Asymmetric transmission, quantified by the Contrast Ratio (CR) [17, 18], measures the difference in transmission for waves incident from opposite directions. In this study, CR is evaluated based on the comparison of two scatterer orientations, with wave incidence from left to right along the x-axis. The 0° orientation corresponds to the ΓX direction in reciprocal space, while the 90° orientation corresponds to the $X'\Gamma$ direction. The CR is given by:

$$CR = \frac{|\mathbb{T}_{0^\circ} - \mathbb{T}_{90^\circ}|}{|\mathbb{T}_{0^\circ} + \mathbb{T}_{90^\circ}|}, \tag{4}$$

where $\mathbb{T}_{0^\circ}$ and $\mathbb{T}_{90^\circ}$ represent the transmission coefficients for the ΓX and $X'\Gamma$ directions, respectively. The CR quantifies the contrast in wave propagation between the two perpendicular orientations of the multiresonant scatterers, with a maximum value of 1 indicating complete suppression of transmission in one orientation and a minimum value of 0 indicating identical transmission in both orientations.

2.1 Numerical Analysis

This section explores the simulation results based on the geometry described in Section 2, focusing on the band structure and transmission of an incident plane wave. The interaction between the Bragg bandgap and HRs yields increased transmission, particularly due to the alignment of the resonators' mouths. The band structure, calculated using finite element analysis with Floquet periodicity conditions, is shown in Fig. 2. The complete Bragg bandgaps for all propagation directions (ΓX, XM, MX', $X'\Gamma$) are shown in gray, while partial bandgaps for 0° (ΓX) and 90° ($X'\Gamma$) are shown in blue and red, respectively.

The transmission ($\mathbb{T}$) is shown adjacent to the band structure. Transmission values close to zero occur at frequencies corresponding to the partial bandgaps for each orientation, highlighting the acoustic switching function

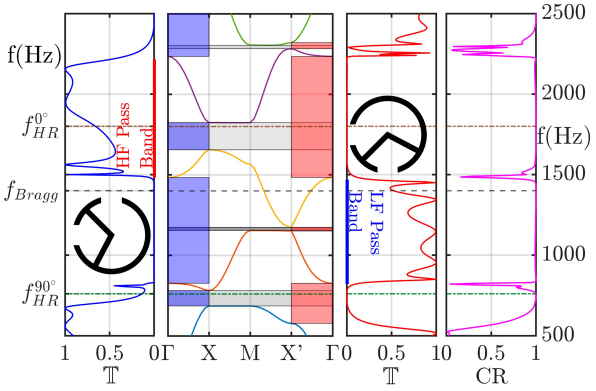

Figure 2. Band structure diagram and perpendicular transmission spectra.

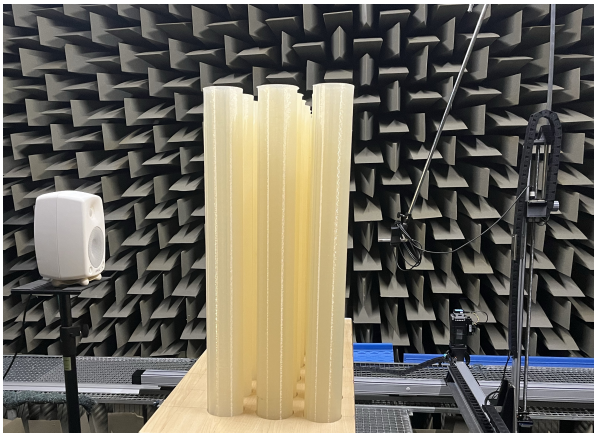

Figure 3. Side view of the experimental setup.

of the structure. The Low Frequency Pass Band (LFPB) spans 830-1500 Hz for the 0° orientation, while the High Frequency Pass Band (HFPB) spans 1500-2250 Hz for the 90° orientation. The first resonant frequencies of the HRs and the central Bragg bandgap frequency (f_{Bragg}) follow the order $f_{\text{HR}}^{90^\circ} < f_{\text{Bragg}} < f_{\text{HR}}^{0^\circ}$, enabling interactions that support the acoustic switch function.

Complete bandgaps, shown in gray, occur at frequencies close to the first resonant frequencies of the HRs ($f_{\text{HR}}^{90^\circ} = 760$ Hz and $f_{\text{HR}}^{0^\circ} = 1800$ Hz) and the Bragg frequency ($f_{\text{Bragg}} = 1400$ Hz). Despite their presence, the SC maintains effective transmission in both the LFPB and HFPB.

2.2 Experimental Assessment

A prototype SC device was manufactured using 3D printing and tested in the anechoic chamber of the Higher Polytechnic School of Gandia (Valencia, Spain). The experimental setup, shown in Fig. 3, included a Genelec 8030A loudspeaker as the sound source and a B&K Type 4189 microphone for acoustic field measurements. The SC was placed on a rigid wooden base, and measurements were taken using a 3D Robotised Acoustic Measurement System.

The frequency range of interest was 500-2500 Hz, with the source placed 0.5 m from the SC. Measurements were taken over a 1.1 m × 0.5 m grid with a spacing of $a/4 = 0.03$ m, resulting in 576 measurement points. The microphone was calibrated using a B&K Sound Calibrator Type 4231, and the robotized system ensured precise acoustic field mapping.

3. RESULTS

The experimental results are compared with numerical simulations in Fig. 4, which shows the transmittance ($\mathbb{T}$) and contrast ratio (CR) as functions of frequency. The top plot illustrates $\mathbb{T}$ for both 0° and 90° orientations, with numerical and experimental data showing strong agreement. The bottom plot depicts CR, highlighting the difference in transmittance between the two orientations. High CR values in the LFPB (830-1500 Hz) and HFPB (1500-2250 Hz) indicate effective acoustic switching behavior.

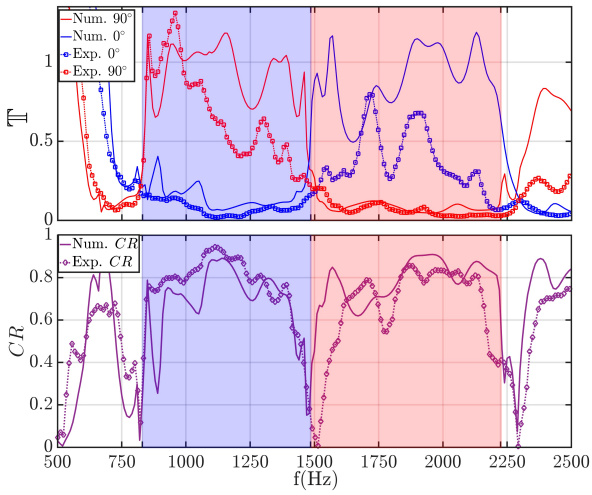

Figure 4. Transmittance, numerical and experimental (top); contrast ratio (CR), numerical and experimental (bottom).

The design functions as an effective acoustic filter, with the ability to control transmission based on scatterer orientation. The strong agreement between numerical and experimental results underscores the robustness of the design and experimental methodology. Fig. 5 shows insertion loss (IL) maps and CR maps for representative frequencies in the LFPB and HFPB, further illustrating the acoustic switching performance of the SC.

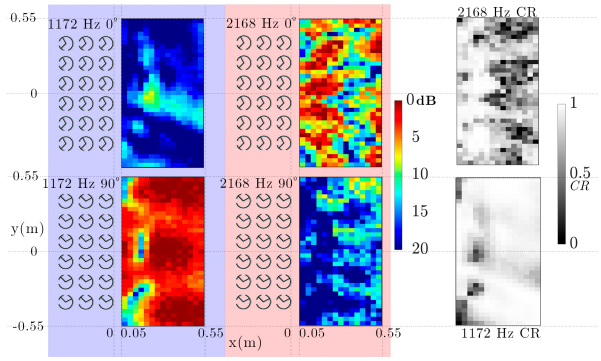

Figure 5. Experimental insertion loss maps with CR maps for two representative frequencies at 0° and 90°.

The results demonstrate the SC's potential as an effective acoustic switch, with tunable transmission properties based on scatterer orientation. This capability is promising for applications in acoustic control, passive filtering, and reconfigurable acoustic devices.

4. CONCLUSION

In conclusion, this paper introduces a novel multiresonant SC device that leverages the interaction between Bragg and Helmholtz resonator-based bandgaps in a simple 3D-printed structure. By varying the scatterer orientation, the device effectively switches between two distinct frequency passbands (830–1500 Hz and 1500–2250 Hz), overcoming limitations of existing acoustic switches that rely on complex geometries or operate at higher frequencies.

The device's performance was validated through numerical and experimental studies, demonstrating strong agreement. Transmission characteristics, contrast ratio (CR), and insertion loss (IL) confirmed its ability to control acoustic response based on scatterer orientation, achieving high contrast and effective attenuation.

Potential applications include urban and industrial noise reduction and adaptive acoustic environments in buildings and vehicles. This versatile and easy-to-implement design opens new possibilities for wave manipulation and acoustic metamaterials.

5. ACKNOWLEDGEMENT

This research was funded by grant PID2022-138321NB-C22 funded by MICIU/AEI/ 10.13039/501100011033 and ERDF/EU. This work was also supported by Construct Innovate, Ireland's National Research Centre for Construction Technology and Innovation (Enterprise Ireland TC-2022-0033, Seed Fund Call CISFC1-23_002). This research was also supported by project "MUD-MADE: MUlti-objective optimization of Digitally MAnufactureD Earth building components supported by neural networks (PRIN PNRR 2022)".

6. REFERENCES

[1] W. E. Kock and F. K. Harvey, "Refracting Sound Waves," *The Journal of the Acoustical Society of America*, vol. 21, pp. 471–481, Sept. 1949.

[2] E. Economou and M. M. Sigalas, "Elastic and acoustic wave band structure," *Journal of sound and vibration*, vol. 158, no. 2, pp. 377–382,, 1992.

[3] C. Kittel, *Introduction to Solid State Physics*. Hoboken, NJ: Wiley, 8th ed ed., 2005.

[4] T. Miyashita, "Sonic crystals and sonic wave-guides," *Measurement Science and Technology*, vol. 16, pp. R47–R63, May 2005.

[5] J. Redondo, R. Picó, V. Sánchez-Morcillo, and W. Woszczyk, "Sound diffusers based on sonic crystals," *The Journal of the Acoustical Society of America*, vol. 134, pp. 4412–4417, Dec. 2013.

[6] D. Ramírez-Solana, V. Sangiorgio, N. Parisi, J. Redondo, A. M. Mangini, and M. P. Fanti, "Parametric Design and Assessment of 3D Printable Open Noise Barrier: Device Customization to Protect Buildings from Train Brake Noise," *Journal of Architectural Engineering*, vol. 30, no. 2, 2024.

[7] J. V. Sanchez-Perez, C. Rubio, R. Martinez-Sala, R. Sanchez-Grandia, and V. Gomez, "Acoustic barriers based on periodic arrays of scatterers," *Applied Physics Letters*, vol. 81, pp. 5240–5242, Dec. 2002.

[8] S. Alagoz and B. Baykant Alagoz, "Sonic crystal acoustic switch device," *The Journal of the Acoustical Society of America*, vol. 133, no. 6, pp. EL485–EL490, 2013.

[9] Z. Liu, X. Zhang, Y. Mao, Y. Y. Zhu, Z. Yang, C. T. Chan, and P. Sheng, "Locally Resonant Sonic Materials," *Science*, vol. 289, pp. 1734–1736, Sept. 2000.

[10] A. Krynkin, O. Umnova, A. Y. B. Chong, S. Taherzadeh, and K. Attenborough, "Scattering by coupled resonating elements in air," *Journal of Physics D: Applied Physics*, vol. 44, p. 125501, Mar. 2011.

[11] J. Redondo, D. Ramírez-Solana, and R. Picó, "Increasing the Insertion Loss of Sonic Crystal Noise Barriers with Helmholtz Resonators," *Applied Sciences*, vol. 13, pp. 3662:1–3662:13, Mar. 2023.

[12] B. Wu, W. Jiang, J. Jiang, Z. Zhao, Y. Tang, W. Zhou, and W. Chen, "Wave Manipulation in Intelligent Metamaterials: Recent Progress and Prospects," *Advanced Functional Materials*, vol. 34, p. 2316745, July 2024.

[13] H. Heo, A. Krokhin, A. Neogi, Z. Cui, Z. Yuan, Y. Hua, J. Ju, and E. Walker, "Multifunctional Acoustic Device Based on a Phononic Crystal with Independently Controlled Asymmetric Rotating Rods," *Physical Review Applied*, vol. 19, p. 054008, May 2023.

[14] L. Brillouin, *Wave Propagation in Periodic Structures*. New York: Dover Publications inc., 1953.

[15] L. E. Kinsler, A. R. Frey, A. B. Coppens, and J. V. Sanders, *Fundamentals of Acoustics*, vol. 72. New York, US: John Wiley & Sons, 2000.

[16] G. P. Ward, R. K. Lovelock, A. R. J. Murray, A. P. Hibbins, J. R. Sambles, and J. D. Smith, "Boundary-Layer Effects on Acoustic Transmission Through Narrow Slit Cavities," *Physical Review Letters*, vol. 115, p. 044302, July 2015.

[17] X.-F. Li, X. Ni, L. Feng, M.-H. Lu, C. He, and Y.-F. Chen, "Tunable Unidirectional Sound Propagation through a Sonic-Crystal-Based Acoustic Diode," *Physical Review Letters*, vol. 106, p. 084301, Feb. 2011.

[18] A. Cicek, O. Adem Kaya, and B. Ulug, "Refraction-type sonic crystal junction diode," *Applied Physics Letters*, vol. 100, p. 111905, Mar. 2012.

[19] J. V. Sánchez-Pérez, D. Caballero, R. Mártinez-Sala, C. Rubio, J. Sánchez-Dehesa, F. Meseguer, J. Llinares, and F. Gálvez, "Sound Attenuation by a Two-Dimensional Array of Rigid Cylinders," *Physical Review Letters*, vol. 80, no. 24, pp. 5325–5328, 1998.